Available online at www.sciencedirect.com
ScienceDirect
Journal of Catalysis 243 (2006) 438–441
JOURNAL OF CATALYSIS
www.elsevier.com/locate/jcat

Research Note

Effects of zeolite channel walls and cation migration on N_2O decomposition energies in Fe/ZSM-5

Carl R.F. Lund *

Department of Chemical and Biological Engineering, University at Buffalo, SUNY, Buffalo, NY 14260-4200, USA

Received 13 June 2006; revised 16 August 2006; accepted 19 August 2006

Abstract

Density functional theory was used to compute minimum energy structures for surface intermediates involved in the catalytic decomposition of N_2O over Fe/ZSM-5. The calculations were performed using a computational cluster containing only 5 tetrahedral zeolite atoms, and then repeated using a cluster with two full 10-membered zeolite rings. The differences between these two sets of calculations suggest that using a larger computational cluster allows the iron cation to occupy a site of higher coordination. This is accompanied by small changes in the computed values of ΔE for the five mechanistic reaction steps of N_2O decomposition. Replicating the final geometry of the smaller cluster within the larger cluster indicated that longer-range interactions with the zeolite channel walls do not significantly affect the energies of the mechanistic steps studied.

Keywords: Density functional theory; Fe/ZSM-5; N_2O decomposition

1. Introduction

Ion-exchanged Fe/ZSM-5 catalysts can present a variety of different types of iron sites including isolated ion-exchanged iron cations, ion-exchanged iron cations in close proximity to other cations (iron or noniron), small clusters of iron oxide, and others. Several of these forms are active for the catalytic decomposition of N_2O. The present note considers only one specific type of site—that where the iron exists as charge-compensating, ion-exchange cations that are not in close proximity to other iron cations. Catalysts with these isolated iron cations have been shown to be active for the decomposition of N_2O into N_2 and O_2 [1,2]. The mechanism of this reaction over iron cation sites has been studied using computational chemistry [3–13]. The work of Heyden et al. appears to be the most comprehensive and definitive study [12,13] for systems with isolated iron cations. Among other findings, the latter study showed that the five-step pathway shown in Table 1 properly predicts the experimentally observed reaction orders and activation energy for nitrous oxide decomposition. Most computational studies of this type model the active site using a small cluster comprising only a few atoms from the zeolite framework. The purpose of the present study was to model the active site using much larger clusters and, by doing so, probe the effects of longer-range interactions between the adsorbed intermediates and the zeolite channel walls and the effects of any movement of the exchanged iron cations on adsorption of different species.

2. Methods

The active site in Fe/ZSM-5 was modeled using clusters of atoms constructed on the basis of the crystallographic structure of ZSM-5 [14]. It has been reported [15,16] that the energy associated with placing an aluminum atom in a tetrahedral site of ZSM-5 varies moderately between the 12 crystallographically distinct tetrahedral locations of ZSM-5, and that the T1 site has the lowest energy. Consequently, the clusters used for calculations here were derived from the crystallographic structure of ZSM-5 wherein the Si at one T1 site was replaced with Al. A high-spin Fe^{3+} cation was used to compensate for the charge imbalance caused by replacing the Si with Al; the additional charges on this iron cation were compensated for by species

* Fax: +1 (716) 645 3822.
E-mail address: lund@eng.buffalo.edu.

0021-9517/$ – see front matter
doi:10.1016/j.jcat.2006.08.014

Table 1
Calculated energies of reaction for the mechanistic steps of N_2O decomposition

Reaction	ΔH (kJ/mol), Heyden et al.	$\Delta E_{(\text{naked})}$ (kJ/mol)	$\Delta E_{(\text{initial})}$ (kJ/mol)	$\Delta E_{(2\text{ ring})}$ (kJ/mol)
$N_2O + FeO \rightarrow N_2O$–FeO	−20.1	−27.7	−49.9	−45.8
N_2O–FeO $\rightarrow N_2 +$ OFeO	−83.7	−73.1	−66.7	−53.2
$N_2O +$ OFeO $\rightarrow N_2O$–OFeO	−5.0	−19.0	−38.9	−49.5
N_2O–OFeO $\rightarrow N_2 +$ O–OFeO	−50.2	−16.6	13.4	4.5
O–OFeO $\rightarrow O_2 +$ FeO	−2.5	−0.9	4.8	6.7

adsorbed on it. Two different cluster models were used to represent the zeolite in the present investigation. The first of these models is small and similar to clusters used in other studies of this system [9,12,13]; henceforth it is referred to as the "naked" cluster.

To generate the naked cluster—the Al atom at the T1 position—the four oxygen atoms bonded to it and the four Si atoms bonded to those oxygen atoms were cut from the crystallographic structure. The Si–O bonds that were broken in doing so were replaced with terminal Si–H bonds. The Si–H bonds had the same direction as the Si–O bonds they replaced, but the Si–H distance was set equal to 0.148 nm. (This Si–H distance was chosen because geometry optimization with the spatial coordinates of the Si atoms held constant resulted in Si–H bond lengths of nearly equal length, with an average value of 0.148 nm.) In geometry optimizations using the naked cluster, the spatial coordinates of the terminal H atoms were held constant while the coordinates of all other atoms were allowed to vary.

The second cluster model henceforth called the "two-ring" cluster, was generated using the same procedure as with the naked cluster except that many more of the zeolite atoms were retained. Specifically, a total of 23 Si atoms (in addition to the Al atom at the T1 position) were retained. The retained Si atoms were selected so that 2 complete 10-membered rings were present about the Al atom. All oxygen atoms bonded to two retained atoms were also retained; oxygen atoms bonded to a single retained Si were replaced with H atoms as in the naked cluster. Altogether, the double 10-ring cluster involved 92 atoms plus the iron cation and the ligands bonded to it. As with the naked cluster, the spatial coordinates of the terminal H atoms were held constant during geometry optimizations, but all other atoms were free to move.

Geometry optimizations and energy calculations were performed using the Jaguar software package [17]. Restricted, open-shell density functional theory was used using B3LYP hybrid exchange-correlation functionals, tight cutoffs, and the finest DFT grid (125 radial shells and an angular offset of 30, giving 434 angular points per shell with no pruning [17]). Symmetry was not imposed during the calculations, and no corrections were used for basis set superposition errors or zero-point energies. For the naked clusters, TVZ** basis sets were used on all atoms. Mixed basis sets were used for the two-ring clusters. For the atoms of the zeolite framework, 3-21G basis sets were used, except as noted later. TZV** basis sets were used on all other atoms. The spin multiplicity was six in all clusters studied here.

Naked cluster geometry optimizations were performed on each of the five surface species appearing in the mechanism of Table 1: the oxide species (Fe–O), the oxo species (O–Fe–O), N_2O adsorbed on the oxide (N_2O–Fe–O), N_2O adsorbed on the oxo (N_2O–O–Fe–O), and O_2 adsorbed on the oxide (O–O–Fe–O). The results of the calculations, together with the results from the calculations on the gas phase species, were used to calculate $\Delta E_{(\text{naked})}$ for each of the five mechanistic steps shown in Table 1. Next, two-ring clusters were generated with all of the atoms in their crystallographic locations except for the Al at the T1 site, the four O atoms bonded to it, and the four Si atoms bonded to them. These were instead placed at the locations determined by geometry optimization of the naked cluster. The ion-exchanged iron cation and the associated adsorbed species were also added, again being located at the positions determined by geometry optimization of the naked cluster. That is, the optimized naked cluster was grafted into a two-ring cluster, and single-point energy calculations were performed to determine $\Delta E_{(\text{initial})}$ for each of the five mechanistic steps, as reported in Table 1. Finally, a full geometry optimization was performed wherein only the terminal H atoms of the two-ring cluster were constrained to remain fixed in space. The results were again used to calculate $\Delta E_{(2\text{ ring})}$ for each of the five mechanistic steps as reported in Table 1.

3. Results and discussion

The (optimized) geometries of the naked cluster and two-ring cluster Fe–O species are shown in Figs. 1a and 1b. As noted, the mechanism in Table 1 was examined in detail by Heyden et al. [12,13], who used a cluster similar to the naked cluster here. Table 1 shows that the present results agree quite well with their work. The computed energy changes for four of the five steps agree within <15 kJ mol^{-1}, and the other differs by 33.6 kJ mol^{-1}. These differences between the two studies can be attributed to placing the aluminum cation at different framework sites (T1 vs T12), differences in the geometry optimization constraints (H positions held constant vs Si positions), and differences in the reported quantity (ΔE uncorrected for zero-point energy vs ΔH).

When the geometries of the optimized naked clusters are grafted into the two-ring clusters, the energies of the adsorbed species might be affected by longer-range interactions with the zeolite channel walls; in addition, strain may be introduced into the both framework and the former naked cluster. Table 1 shows that the net effect is quite small, however. The ΔE values calculated for the five mechanistic steps using the naked cluster

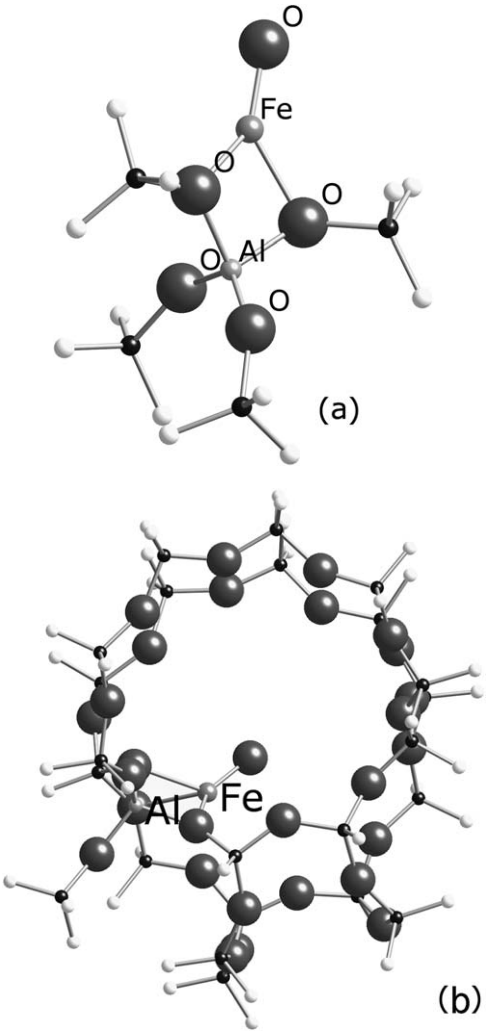

Fig. 1. Optimized geometry of the Fe–O intermediate of Table 1 for (a) the naked cluster and (b) the two-ring cluster. The unlabeled small white atoms are hydrogen, small black atoms are silicon, and larger unlabeled atoms in (b) are oxygen.

Table 2
Change in energy upon optimization of the geometry of the two-ring cluster intermediates

Species	ΔE (kJ/mol)
FeO	−294.3
N_2O–FeO	−290.2
OFeO	−276.7
N_2O–OFeO	−287.3
O–OFeO	−296.1
No cation	−265.4

In all cases involving an iron cation, it is modeled as high-spin Fe^{3+} and the cluster model includes one Al^{3+} in a T1 lattices site; in the case without an iron cation, all tetrahedral zeolite cations were Si cations.

change by 30 kJ mol^{-1} or less on initial grafting into the two-ring clusters.

Subsequent geometry optimizations of the initial two-ring clusters are expected to relieve, as much as possible, strains resulting from insertion of the naked geometry into the two-ring cluster. Table 2 shows that the calculated energies of the individual species each decreased by slightly less than

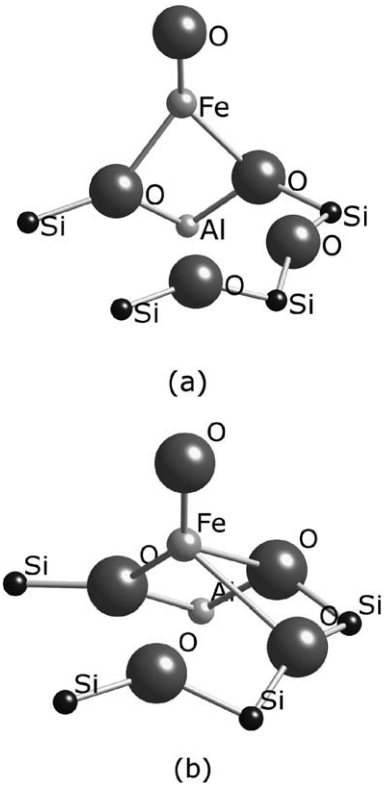

Fig. 2. Portions of the two-ring cluster showing the coordination of the Fe–O intermediate of Table 1 (a) as initially grafted in from the optimized naked cluster geometry and (b) after geometry optimization.

300 kJ mol^{-1}. It appears that most of the decrease in each species' energy can be attributed to relieving strain in the zeolite lattice, because, as also shown in Table 2, an all-silicon two-ring cluster (without aluminum or iron cations) experienced an energy decrease of ca 265 kJ mol^{-1}.

If one assumes that the strain in each of the initial two-ring clusters is comparable, the net remaining decrease of the intermediates' energies is on the order of 10–30 kJ mol^{-1}. This is consistent with Table 1, which shows that the calculated ΔE for each of the five mechanistic steps changed by $<$15 kJ mol^{-1} relative to the initial two-ring cluster and by ca $<$30 kJ mol^{-1} relative to the naked cluster. At the level of theory used in these calculations, one might expect an error on the order of 12–15 kJ mol^{-1} [18]. Therefore, it would seem, at least for the system studied here, that very little is gained by using the larger computational clusters, at least with respect to the energies of reaction. In addition to longer-range interactions between the surface intermediates and the zeolite channel walls, these small changes may also be attributed, in part, to migration of the iron cation to lower-energy locations that simply did not exist in the naked cluster.

Using the larger clusters creates additional locations for the ion-exchanged cation to reside. Although the overall energetic differences are minimal, there are clear differences in the geometries of the sites. Fig. 2 shows the migration of the iron cation of the Fe–O species when the two-ring cluster is used. Optimization of the naked cluster for Fe–O generates an iron cation with an unusual three-fold coordination, as shown

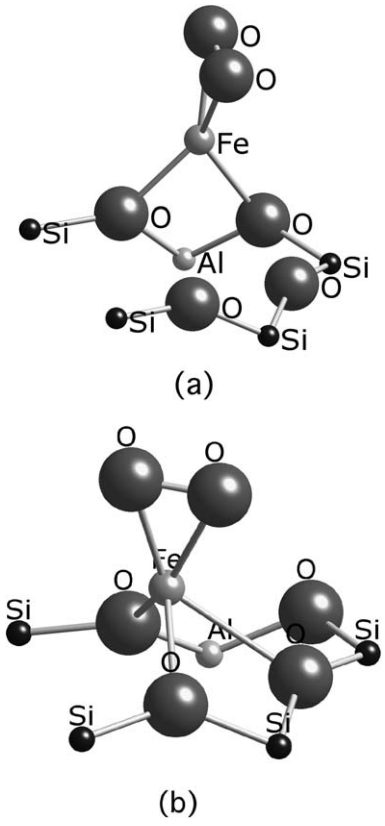

Fig. 3. Change in the iron cation coordination upon optimization of the O–Fe–O intermediate: relevant portion of (a) the initial two-ring structure and (b) the optimized two-ring structure.

in Fig. 1a. When placed into the two-ring cluster (Fig. 2a) and allowed to find a lower-energy conformation, the cation moves closer to two additional framework oxygen atoms, as shown in Fig. 2b. In doing so, both of the original bonds from the iron cation to lattice oxygen atoms lengthen (from 0.205 to 0.225 nm and from 0.202 to 0.205 nm), and the distances from the iron to the two additional lattice oxygen atoms become 0.245 nm and 0.262 nm. The bond distance between the iron cation and the nonframework oxygen is 0.166 nm in both cases.

The intermediate species with the greatest change in coordination is the O–Fe–O species of Table 1. The initial and final structures are shown in Fig. 3, which shows that the iron cation becomes more closely coordinated to two new oxygen atoms while migrating away from one of the original oxygen atoms to which it was coordinated. Nonetheless, it is apparent from Table 1 that the final energy change associated with cation migration is of negligible magnitude. In the present study, the activation barriers associated with the mechanistic steps were not determined.

It is perhaps important to note that when the two-ring cluster was used, some care had to be exercised with respect to basis set selection. In the earliest calculations with the two-ring cluster, all of the framework atoms except those in common with the naked cluster used 3-21G basis sets. Migration of the cation, like that shown above, in these earliest calculations resulted in coordination of the iron to framework atoms using the less-complete 3-21G basis set. This could affect the final location of the cation and also introduce inaccuracies. Therefore, the final geometry optimizations were repeated using TZV** basis sets on the framework atoms in the vicinity of the iron cation (i.e., on the four Si atoms, the four framework O atoms and Al atom shown in Figs. 2 and 3). The results presented in Tables 1 and 2 are based on these final calculations.

4. Conclusion

Computed values of ΔE for the five mechanistic reaction steps of N_2O decomposition changed slightly when much larger computational clusters were used in place of minimally sized clusters. Calculations with even larger clusters will be needed to show that the large cluster results represent a converged solution that will not change further with increased cluster size. Nonetheless, the current results suggest, at least for Fe/ZSM-5 and the mechanistic pathway studied, that longer-range interactions between surface species and the zeolite channel wall are relatively unimportant. It also suggests that the exact geometry of the cation exchange site has only a minor effect on the reaction energetics, because the siting of the cations changed when the larger clusters were used, but the energies of the mechanistic steps changed little. Thus, for the system studied here, using the naked cluster is sufficiently accurate for calculating energies of reaction. Larger clusters are preferred for calculating the geometries of the sites.

Acknowledgments

This material is based on work supported in part by the National Science Foundation (Award CTS-0099359). The donation of the SunFire computers used in the final DFT calculations by Sun Microsystems is gratefully acknowledged, as is the use of facilities at the Center for Computational Research at the University at Buffalo, SUNY.

References

[1] C. Sang, B.H. Kim, C.R.F. Lund, J. Phys. Chem. A 109 (2005) 2295.
[2] B.R. Wood, J.A. Reimer, A.T. Bell, J. Catal. 209 (2002) 151.
[3] A.L. Yakovlev, G.M. Zhidomirov, R.A. van Santen, J. Phys. Chem. B 105 (2001) 12297.
[4] A.V. Arbuznikov, G.M. Zhidomirov, Catal. Lett. 40 (1996) 17.
[5] A. Chatterjee, A.K. Chandra, J. Mol. Catal. 119 (1997) 51.
[6] R. Vetrivel, S. Pal, S. Krishnan, J. Mol. Catal. 66 (1991) 385.
[7] K. Yoshizawa, Y. Shiota, T. Yamabe, J. Phys. Chem. 104 (2000) 734.
[8] K. Yoshizawa, T. Yumura, T. Yamabe, Bull. Chem. Soc. Jpn. 73 (2000) 29.
[9] J.A. Ryder, A.K. Chakraborty, A.T. Bell, J. Phys. Chem. B 106 (2002) 7059.
[10] N.A. Kachurovskaya, G.M. Zhidomirov, E.J. Hensen, R.A. van Santen, Catal. Lett. 86 (2003) 25.
[11] E.J. Hensen, Q. Zhu, R.A. van Santen, J. Catal. 220 (2003) 260.
[12] A. Heyden, A.T. Bell, F.J. Keil, J. Catal. 233 (2005) 26.
[13] A. Heyden, B. Peters, A.T. Bell, F.J. Keil, J. Phys. Chem. B 109 (2005) 1857.
[14] D.H. Olson, G.T. Kokotallo, S.L. Lawton, W.M. Meier, J. Phys. Chem. 85 (1981) 2238.
[15] U. Eichler, M. Brandle, J. Sauer, J. Phys. Chem. B 101 (1997) 10035.
[16] D. Nachtigallova, P. Nachtigall, M. Sierka, J. Sauer, Phys. Chem. Chem. Phys. 1 (1999) 2019.
[17] Jaguar, Schrödinger, LLC, New York, NY, 2005.
[18] B.J. Lynch, D.G. Truhlar, J. Phys. Chem. A 105 (2001) 2936.